Liquid Crystals
Publication details, including instructions for authors and subscription information:
http://www.informaworld.com/smpp/title~content=t713926090

Characteristic times in the homeotropic to planar transition in cholesteric liquid crystals

P. Watson; V. Sergan; J. E. Anderson; J. Ruth; P. J. Bos

Online publication date: 06 August 2010

To cite this Article Watson, P. , Sergan, V. , Anderson, J. E. , Ruth, J. and Bos, P. J.(1999) 'Characteristic times in the homeotropic to planar transition in cholesteric liquid crystals', Liquid Crystals, 26: 5, 731 — 736
To link to this Article: DOI: 10.1080/026782999204813
URL: http://dx.doi.org/10.1080/026782999204813

LIQUID CRYSTALS, 1999, VOL. 26, NO. 5, 731–736

Characteristic times in the homeotropic to planar transition in cholesteric liquid crystals

P. WATSON*, V. SERGAN, J. E. ANDERSON, J. RUTH and P. J. BOS
Liquid Crystal Institute, Kent State University, Kent, OH 44242, USA

(*Received 5 October 1998; accepted 23 December 1998*)

The effect of surfaces on the relaxation from the homeotropic state to the planar state of cholesteric liquid crystals is investigated. By using an optical retro-reflection technique, the orientation and pitch of cholesteric helices as a function of time have been isolated for various surface treatments. It is found that the pitch relaxes to its minimum value in a matter of milliseconds, independent of surface treatment. Secondary pitch relaxations take place after this. The time dependence of the angular distribution of helical axes is also found to be complex, operating on several time scales.

1. Introduction

It is well established that the relaxation of cholesteric liquid crystals from the homeotropic (H) state to the planar cholesteric (P) state involves a conical relaxation to a metastable long-pitch Grandjean state known as the transient planar (TP), followed by the evolution of the equilibrium state [1–4]. This relaxation is commonly given a characteristic relaxation time of about 200 ms [5], based on optical reflection observations at an oblique angle using a diffuse light source. However, a single characteristic time is not sufficient to describe the complex dynamics of this very rich transition. In this study, we characterize the time scales of the various relaxation processes using experimental techniques.

Yang and Lu derived the elastic free energy of a cholesteric system during the H to TP relaxation from the Frank–Oseen equation as a function of the polar angle and the chirality, and have theoretically estimated and experimentally determined the TP pitch to be approximately $P_0 K_{33}/K_{22}$ [6]. Here, P_0 is the equilibrium planar pitch, K_{22} the twist elastic constant, and K_{33} the bend elastic constant for the liquid crystal material. Their derivation assumes a conical relaxation to TP.

The transient planar is not, however, a stable state. Assuming it to be a perfect Grandjean state, the elastic twist energy of the TP may be written as:

$$f_{\text{twist}} = 2\pi^2 \left(\frac{K_{22}}{P_0^2}\right)\left(1 - \frac{K_{22}}{K_{33}}\right)^2$$

In order to alleviate this high elastic energy, the material undergoes a transition to the planar state. In this study, we will occasionally refer to what has historically been called the 'planar' state as the 'cholesteric' state, because of its non-planar nature, and to avoid confusion with planar surface alignments.

Cholesteric liquid crystals can reflect light through Bragg reflection, because the cholesteric helix is a periodic structure. Light of a wavelength (inside the material) equal to the pitch of the liquid crystal is reflected, providing that it has circular polarization of the same twist sense as the helix, and that the light propagation direction is along the helical axis. Helical axes tipped by an angle θ from the incident light will reflect light with a shorter wavelength, as $\lambda_{\max} = nP \cos\theta$, where n is the average index of refraction of the material [7]. Light of the opposite circular polarization is not reflected. Maximum reflection is obtained in samples with greater than about 5 full pitches of the cholesteric helix [8].

2. Experimental

To determine the orientation of helical axes in a cholesteric material, Khan *et al.* [9] developed an experimental system using a fixed collimated light source and a movable detector. Taheri *et al.* [10] have pointed out the advantages of an experimental system where only light reflected directly back toward a collimated source is detected. In this case, light is detected only from cholesteric domains with helical axis parallel to the direction of detection, with reflective wavelength $\lambda_{\max} = nP$ [7]. We have developed such a system, incorporating sub-millisecond time resolution.

As may be seen in figure 1, our experimental apparatus consists of three systems of standard components. These include a light source (1), a block of electronic components (2), and a block of optical components (3). The light source includes a high power halogen lamp focused

* Author for correspondence; e-mail: phil@scorpio.kent.edu

Journal of Liquid Crystals ISSN 0267-8292 print/ISSN 1366-5855 online
http://www.tandf.co.uk/JNLS/lct.htm
http://www.taylorandfrancis.com/JNLS/lct.htm

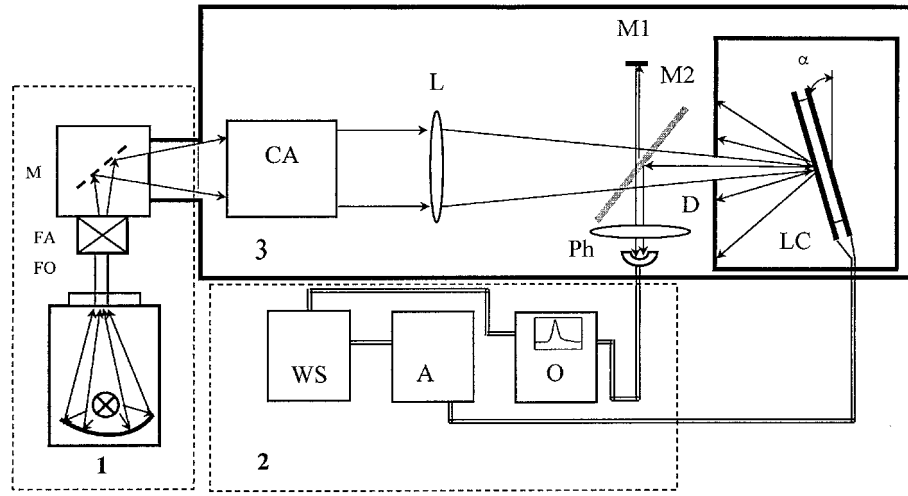

Figure 1. Experimental arrangement.

on the input of a fibre optic light guide (FO), a focusing assembly (FA) and an Oriel Multispec monochromator (M). The block of optical components is placed in a black box, and includes a collimating assembly (CA) which produces a nearly parallel beam of monochromatic light, a long focal length lens (L), a semitransparent mirror (M2), an aluminum mirror (M1), and a rotating liquid crystal cell holder. The block of electronic components includes a Stanford Research Systems digital DS345 Synthesized Function Generator (WS), a 120 V bipolar amplifier (A), a four channel digitizing Tektronix TDS420A oscilloscope (O), and a photodiode (Ph) as a reflected light detector. The voltage applied to the sample is a 45–50 V_{pp} a.c. 1 kHz signal modulated by a 1 Hz square waveform (100% amplitude modulation). Both the modulation and function signals are produced by WS. The output signal of Ph is monitored by the oscilloscope when the modulation is low.

Two independent factors determine the angular resolution of the optical block. These are the divergence of the beam of light (with angle $\sim 5°$) used for cell illumination, and the physical dimensions of the diaphragm D and the spot of light on the cell surface. Physical measurements of the angular resolution (using a mirror in place of the cell) suggest that the true angular resolution is $\pm 2°$.

In order to ensure that the signal is properly normalized, light reflected from mirror M1 is measured at each wavelength when the cell is in the homeotropic state (before the field is removed). This signal, which we will refer to as the 'normalization signal,' gives the wavelength dependence of the light source, monochromator, and detector. During relaxation, the signal measured by the photodiode includes reflections from the cell as well as from the mirror; that is, $M = C + N$, where M is the total measured signal, C corresponds to signal from light reflected from the cell, and N is the normalization signal. This measured signal at each wavelength is divided by the normalization signal, and unity is subtracted from this quotient to give the recorded signal, $R = (M/N) - 1 = [(C + N)/N] - 1 = C/N$. This ensures that all wavelengths for a cell at a specific angle are equally weighted. Because the entire optical system is enclosed in a shielding box, background light noise is negligible.

Cells used in this study had 5 μm cell gaps, and were filled with a mixture of Merck liquid crystal 18349 and CB15 chiral additive, with a maximum equilibrium reflection at about 640 nm. Surface treatments included a strong homeotropic surfactant (Aldrich octadecyltrichlorosilane, which will be referred to as 'silane'), a homeotropic polyimide (Nissan 7511), an unrubbed planar polyimide (Dupont 2555), and a rubbed planar polyimide (Dupont 2555). We will focus primarily on the rubbed planar and strong homeotropic surfaces, these being sufficient to illustrate which aspects of the relaxation are influenced by surface properties.

3. Results

From the measured optical response at various wavelengths for a cell, a 3-dimensional graph of reflected intensity vs. wavelength and time for the data can be constructed. Figure 2(*a*) represents the initial relaxation process for a cell with a strong planar (rubbed 2555) alignment. Light was incident on the sample at an angle $\alpha = 5°$ from the cell normal direction. From Snell's law, with an average index of refraction of 1.6 for the host liquid crystal, this corresponds to helices tilted $3.0° \pm 1.7°$ from the cell normal direction. Note that the TP and P peaks are clearly apparent in this graph. The TP reaches its maximum reflectance at 1.3 ms, fading to zero by 3 ms. The P reflection grows more slowly, reaching its maximum of 4.8 a.u. on our scale for this angle at about 900 ms, well outside the range of this plot.

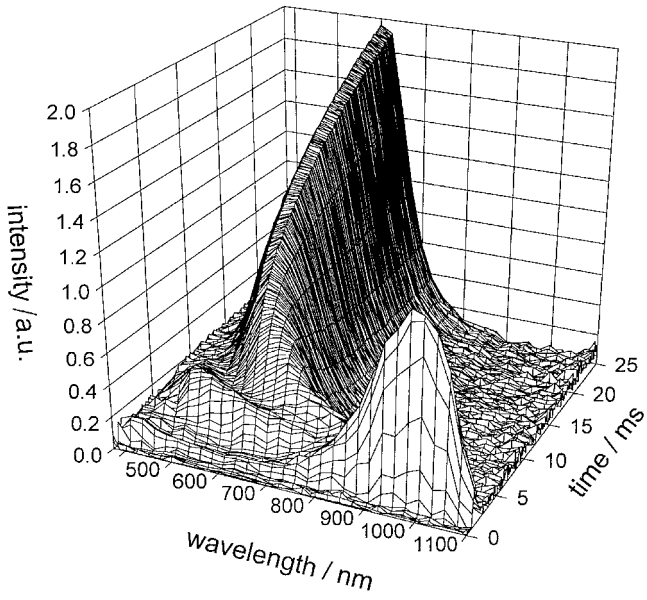

(*a*)

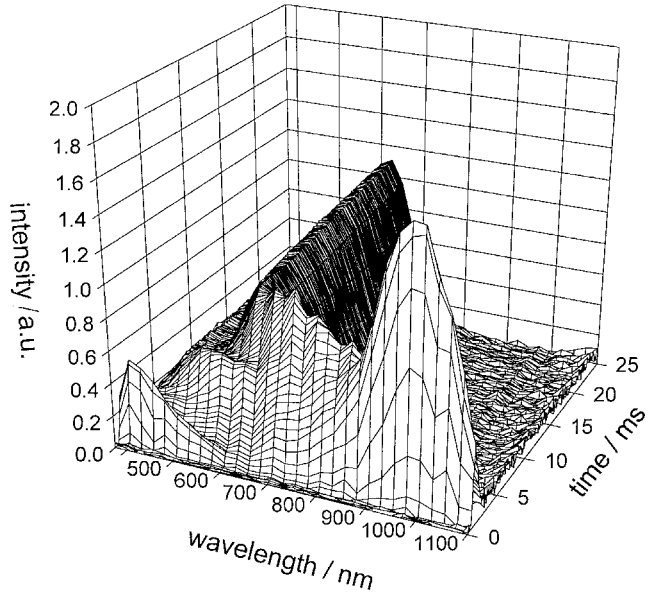

(*b*)

Figure 2. Optical response vs. wavelength and time for (*a*) planar cell, (*b*) homeotropic cell.

Figure 2 (*b*) shows similar observations on the silane cell. Again, the TP and P peaks are clearly apparent. In the relaxation from the TP to P state, the measured brightness reached 70% of its maximum value for this angle in 10 ms. The maximum reflection from this cell at this angle was 1.4 a.u., occurring at 210 ms.

If we plot the wavelength of maximum reflection (λ_{max}) against time for $\alpha = 5°$, we find that the relaxation to a pitch corresponding to a maximum reflection at about 630 nm is completed in about 5 ms (figure 3) for both surface. To see changes in the helical axis distribution, the reflected intensity integrated over all measured wavelengths (data was summed from 375 to 1100 nm, with a bin size of 25 nm, and divided by the number of wavelengths) at various times in the relaxation as a function of α is shown in figure 4. The TP reflection at small angles is somewhat brighter than that at larger angles. During the transition time, the reflected intensity takes on a much wider angular distribution. The distribution for the silane cell remains somewhat peaked at small angles, while that of the planar cell is largely flat.

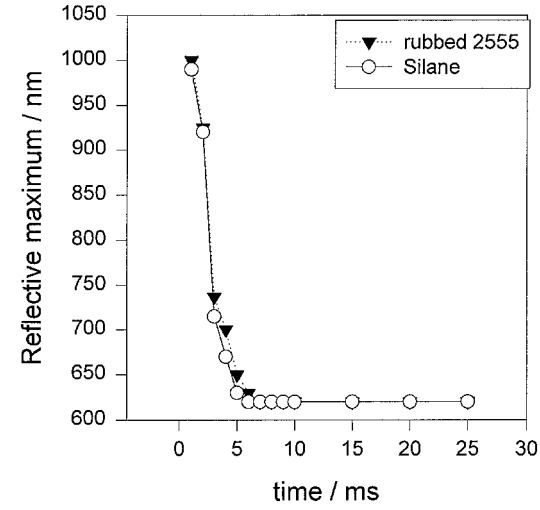

Figure 3. Reflective maximum vs. time for $x = 5°$ for planar and homeotropic cells.

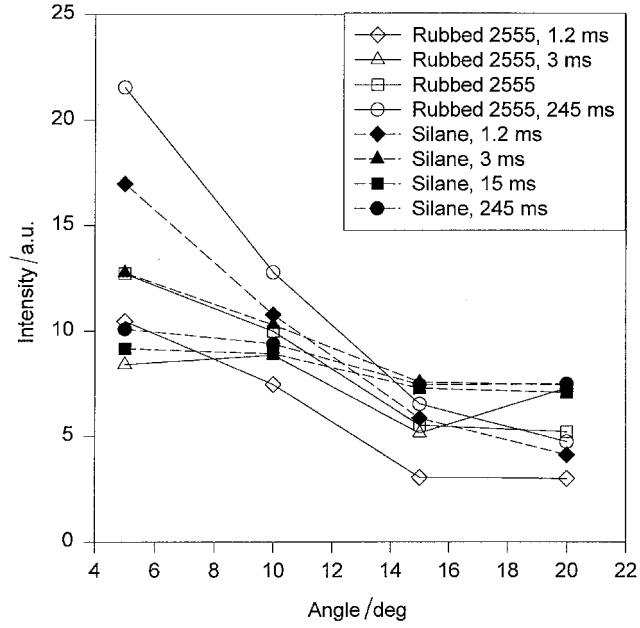

Figure 4. Reflective intensity vs. α, for planar and homeotropic cells.

In the P state, the angular distribution for the silane cell remains wide, while that for the rubbed 2555 cell becomes highly peaked.

On looking at the same relaxation continuing out to 20 s, other effects are seen. Figure 5(*a*) shows the measured response from the rubbed 2555 cell at wavelengths ranging from 525 to 675 nm with $\alpha = 5°$. Note that the reflectance at longer wavelengths tends to fall off more gradually than at shorter wavelengths. Figure 5(*b*) shows the reflectance from the silane cell at various wavelengths with $\alpha = 5°$. Note how the longer wavelengths have a complex reflectance curve, rising quickly to a peak, then decreasing somewhat before rising again. This type of relaxation curve has been reported several times previously [5, 11].

In order to determine the cause of the complex curves in figure 5, we wish to separate the effects of pitch variation and helical axis reorientation. Examination of the intensity integrated over wavelength provides a picture of changes in the total reflection at various angles as a function of time (figure 6). These graphs represent the intensity integrated from 500 to 700 nm with a bin size of 25 nm. The values from all bins are summed, and the sum is divided by the number of bins. The data are expected to be closely related to the density of helical axes along the measured direction (corrected for refraction). Notice that the reflection increases with time at larger

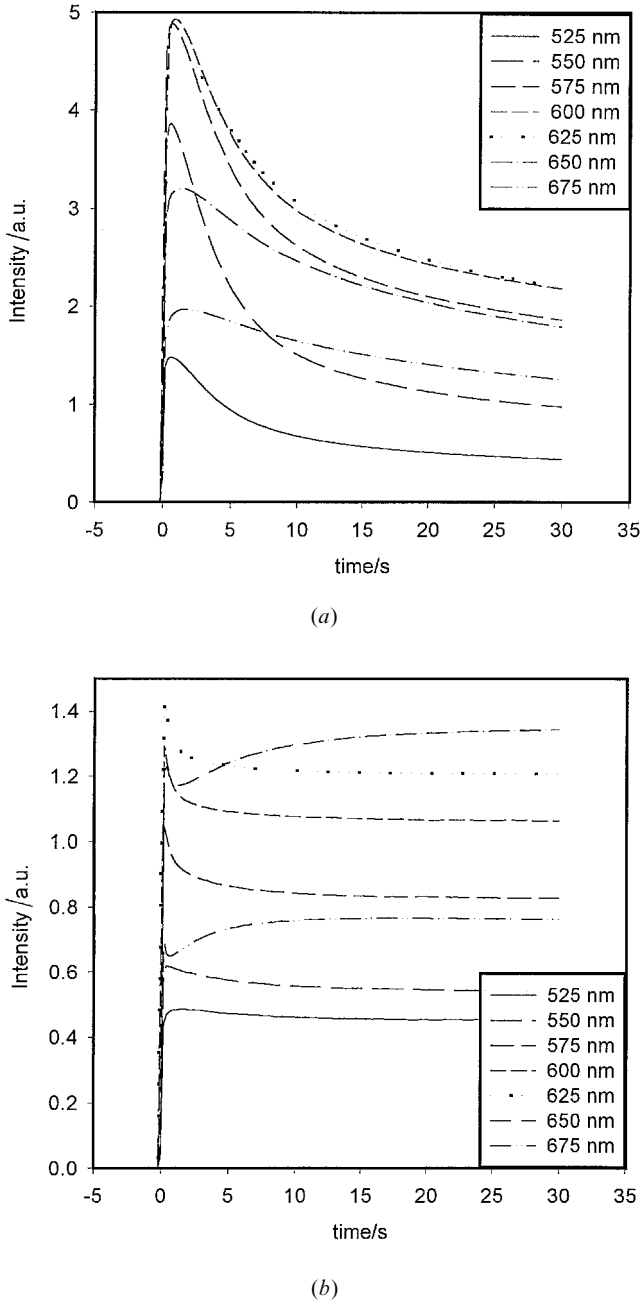

Figure 5. Reflective intensity vs. time for $\alpha = 5°$: (*a*) planar cell, (*b*) homeotropic cell.

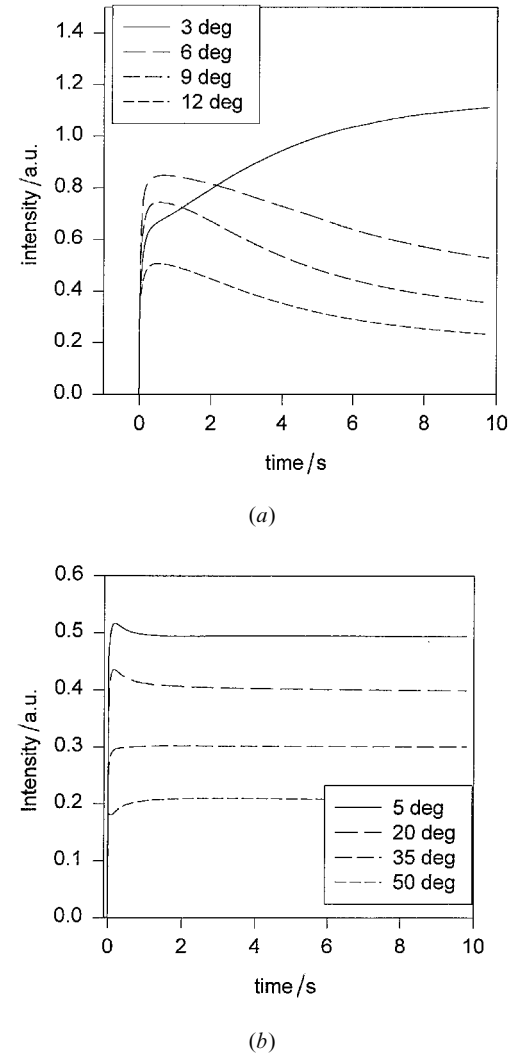

Figure 6. Integrated reflective intensity vs. time: (*a*) planar cell, (*b*) homeotropic cell.

angles for the silane cell, while it increases and then decreases at small angles. We wish to have a formulaic representation of the decrease in intensity at $\alpha = 5°$ for the silane cell for numerical calculations to be explained below. We found that the shape of the integrated reflectance response of the silane cell at $\alpha = 5°$ after a time of 200 ms may be fit as $f(t) = 0.493 + 0.0394 \times \exp(-2.499t)$, with a standard error of 0.0003. For the rubbed planar cell, the reflection intensity vs. time increases only at very small angles, while it decreases for all other angles. (Remember that the 3° reflection refers to cholesteric helices $2° \pm 1.7°$ from the substrate normal direction. Also note the different time scales over which these reorientations of helices take place.)

To determine how the pitch is changing as a function of time, we observed the wavelength of maximum reflectance at $\alpha = 5°$ as a function of time, now over times up to 10 s. The maximum reflected wavelength for both samples decreased to 628 nm in about 5 ms before increasing to its final value of 640 nm in about 10 s. This third modification of wavelength was gradual until about 1 s, after which λ_{max} increased approximately logarithmically, fit as $g(t) = 631 + 9.42 \times \exp[-0.551(t-1)]$, with a standard error of 0.47.

4. Discussion

Considering these data, the following observations can be made about the relaxation. The liquid crystal, initially in a homeotropic nematic configuration, relaxes to a transient planar state with pitch equal to $P_0 K_{33}/K_{22}$ in about 1.3 ms, independent of the surface alignment used. From the transient planar, the material undergoes a second relaxation to a pitch somewhat shorter than P_0 (see above). It is particularly interesting to note that the approximate equilibrium pitch is obtained in 5 ms, independent of surface alignment.

The main effect of surface treatment is on the orientation of helical axes of the P state. During the relaxation from TP to P, the helical axes become widely distributed, with a slightly wider distribution for the cell with planar alignment. As time increases, the helical distribution of the silane cell widens somewhat over a period of 2 s, while for the rubbed 2555 cell, the helical distribution becomes very narrow, producing a mirror-like reflective state after about 20 s.

Now, consider the longer time scale effects shown in figure 5(*b*). We believe that the complex curves seen at wavelengths greater than 625 nm may be explained as a result of a third relaxation of the pitch (described above) combined with a relaxation in the helical axis distribution. To test this hypothesis, we have reconstructed the intensity vs. time curves for the silane cell at $\alpha = 5°$ from information gathered on these two relaxations and a knowledge of the dependence of the reflected intensity on wavelength.

Our method of reconstructing the data is as follows. First, we take the reflection spectrum from the silane cell at a particular time, then fit this spectrum to a mathematical expression with a parameter λ_{max} corresponding to the peak wavelength of the spectrum. It is necessary to have the spectrum as a function of λ_{max} because λ_{max} will be varied in time to simulate the observed change in pitch. The shape of the experimentally measured spectrum does not change significantly after the first second of the relaxation, even though the position of the curve along the wavelength axis changes considerably. Thus, sliding the spectrum in time by varying λ_{max} provides a reasonable approximation of the observed pitch relaxation. $\lambda_{max}(t)$ is set to the experimentally observed values (that is, an analytical fit to the change in wavelength of maximum reflection) as described above. At this point in the reconstruction process, we have a mathematical expression for the reflection as a function of time and wavelength, taking into account the observed change in pitch, but neglecting the observed change in helical axis distribution. In order to take variations in reflection due to changes of the helical axis distribution into account, we multiply the amplitude of the reflection at each time t and wavelength λ with the value of the curve corresponding to a decrease in brightness due to changes in the helical axis distribution at that t. Details of this process will be described in the next paragraph.

The mathematical expression for the reflection spectrum of silane at $\alpha = 5°$ and at an arbitrary time (1 s) was obtained by fitting the measured spectrum to a summation of three gaussians, as

$$h(\lambda, \lambda_1) = 0.219 + 0.7774 \exp\left[-0.5\left(\frac{\lambda - \lambda_1 + 18}{55.6}\right)\right] + 0.28 \exp\left[-0.5\left(\frac{\lambda - \lambda_1 - 12}{23.6}\right)\right] + 0.054 \exp\left[-0.5\left(\frac{\lambda - \lambda_1 + 55}{15.6}\right)\right]$$

A value of 0.02 was obtained for the rms difference between this formula and the measured spectrum. Note that this approximation is not meant to provide any insight into the nature of the reflection spectrum, but merely to provide a formulaic representation of the reflection spectrum (with respect to the reference point λ_1) for ease of numerical manipulation. Once this fit was determined, the maximum wavelength λ_1 in the obtained function was replaced with a function $\lambda_{max}(t)$, defined as 631 nm at times less than 1 s, and as $g(t)$, the exponential fit to the data from the third pitch relaxation, at times greater than 1 s, as described in the previous

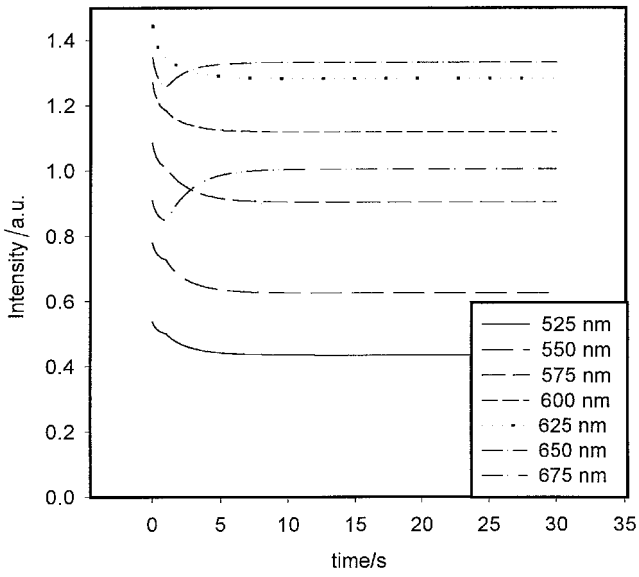

Figure 7. Calculated reflective intensity vs. time curves.

section. This substitution resulted in a surface $A_1(\lambda, t)$ in a space with coordinates of wavelength, time, and amplitude. The obtained surface represents the reflectance spectrum of the material as a function of time, ignoring the effects of changes in helical axis distribution. The helical axis reorientation was then introduced to this function by multiplying the amplitude values with the exponential fit to the measured amplitude decrease, $f(t)$, for $\alpha = 5°$ described in §3 above. The amplitude of this new surface $A_2(\lambda, t)$ was then multiplied by a constant factor of 2.28 to adjust our amplitude to fit better that of the data. The curves shown in figure 7 are $y = 2.28A_2(\lambda, t)$; that is, $y = 2.28f(t)h[\lambda, \lambda_{\max}(t)]$; at various fixed λ. On comparing these curves with those shown in figure 5(*b*), the close correlation of the graphs suggests that the unusual shape of the reflection curves for the silane cell is due to two separate processes. The initial decrease in the intensity of the reflection curve at 650 nm is therefore due to the reorientation of the helical axis distribution to wider angles, and the subsequent rise is related to the change in reflective maximum to a longer wavelength.

5. Conclusions

By using an experimental set-up that measures only retro-reflections from a sample, we have isolated the dynamics of pitch change from the dynamics of the distribution of cholesteric helical axes. Doing so has enabled us to determine much about the nature of the relaxation from the homeotropic state to the planar state (via the transient planar state), and the effects of surfaces on this relaxation. In particular, we have found that the surfaces do not have a significant effect on the time for the pitch to change from the transient planar state to the planar state. For cells with very different surface conditions, the time for the equilibrium pitch to be observed was about 5 ms. The primary effect of the surfaces at times less than 1 s was on the distribution of helical axes in the cell. Additionally, we have used the retro-reflection technique to demonstrate that, the unusual curves that are often observed at longer time scales in cells with homeotropic surface anchoring, can be explained as resulting from a slow change in helical axis distribution combined with an unexpected slow change in the pitch of the material.

We thank Hugh Wonderly for supplying the empty cells. This work was funded by DARPA N61331-96-C-0042.

References

[1] Ohtsuka, T., and Tsukamoto, M., 1973, *Jpn. J. appl. Phys.*, **12,** 22.
[2] Kashnow, R. A., Bigelow, J. E., Cole, H. S., and Stein, C. R., 1974, *Liquid Crystals and Ordered Fluids*, Vol. 2, edited by J. F. Johnson and R. S. Porter (New York: Plenum Press), p. 483.
[3] Kawachi, M., Kogure, O., Yoshii, S., and Kato, Y., 1975, *Jpn. J. appl. Phys.*, **14,** 1063.
[4] Kawachi, M., and Kogure, O., 1977, *Jpn. J. appl. Phys.*, **16,** 1673.
[5] Lu, M.-H., 1997, *J. appl. Phys.*, **81,** 1063.
[6] Yang, D.-K., and Lu, Z.-J., 1995, *SID Digest*, Vol. XXVI, p. 351.
[7] De Gennes, P. G., and Prost, J., 1993, *The Physics of liquid Crystals*, 2nd Edn. (Oxford: Oxford Science Publications), p. 268.
[8] St. John, W. D., Fritz, W. J., Lu, Z. J., and Yang, D.-K., 1995, *Phys. Rev. E.*, **51,** 1191.
[9] Khan, A., Huang, X.-Y., Stefanov, M. E., Bos, P., Davis, D., Taheri, B., and Ruth, J., 1996, *SID Digest*, Vol. XXVII, p. 607.
[10] Taheri, B., Doane, J. W., Davis, D., and St. John, W. D., 1996, *SID Digest*, Vol. XXVII, pp. 39–42.
[11] Gandhi, J. V., Mi, X.-D., and Yang, D.-K., 1998, *Phys. Rev. E.*, **57,** 6761.